Proceedings of the Canadian Society for Mechanical Engineering International Congress 2021
CSME Congress 2021
June 27-30, 2021, Charlottetown, PE, Canada

A Computer Stereo Vision Method for Regional Dynamic Compliance Measurement during Ex-Vivo Lung Perfusion

Jason Der[1], Katie Cameron[2], Steven Cruz Antunes[2], Calvin Jee[2], Reza Sabbagh[1], David S. Nobes[1*]
[1]Department of Mechanical Engineering, University of Alberta, Edmonton, Canada
[2]Tevosol Inc., Edmonton, Canada
Email: dnobes@ualberta.ca

Abstract— Lung transplantation is an advanced treatment available for end-stage respiratory illnesses. Unfortunately, a portion of the donor pool is rejected due to uncertainty about the lung's state of health. Ex Vivo Lung Perfusion (EVLP) is a preservation technique that monitors donor lung performance at a near-physiological state. Performance metrics obtained from the EVLP system are used to evaluate donor lung transplant viability. A computer stereo vison method is proposed to measure region-specific metrics to improve lung performance evaluation. This method monitors donor lung distension, tidal volume, and dynamic compliance. A mechanical lung under ventilation was measured to evaluate the stereo vision method. This method is being developed as a lung transplant evaluation tool.

Keywords: Computer Stereo Vision, Ex Vivo Lung Perfusion, Regional Dynamic Compliance, Non-Invasive Plethysmography

I. INTRODUCTION

Lung transplantation remains the best treatment option for end stage severe pulmonary conditions, such as pulmonary fibrosis caused by SARS-COVID-2 [1]. Unfortunately, this treatment option is underutilized in part due to high rates of donor lung rejection over concerns of transplant viability. Surgeons have poor access to information used to evaluate the donor lungs after procurement , but prior to transplantation, which leads to conservative donor organ rejections. A potential solution to this underutilization is to monitor the donor lung during preservation.

Ex-Vivo Lung Perfusion (EVLP) is a preservation technique that monitors the donor lung's performance metrics at a near physiological state, maintained through mechanical ventilation and perfusion. In preclinical trials, it has demonstrated the potential for extended preservation periods, while improving the lung's state of health. Also, it has been used as an evaluation tool, as measurements can be presented to surgeons prior to transplantation as indicators of transplant viability [2]–[5]. However, EVLP introduces the risk of damaging the lungs due to overinflation. Conversely, underinflation would cause the collapse of alveoli and lead to hypoxia [6]. Proper ventilation avoids overinflation and achieves full lung recruitment. However, the current method of using flow sensors to monitor tidal volume cannot identify localized overinflation and underinflation.

It is hypothesized that a camera-based system could provide region-specific measurements of the lung to improve the quality of information available to assess transplant viability. The proposed method could identify regions of overinflation and lung de-recruitment to allow medical professionals to optimize ventilation settings. This paper outlines the proposed method and preliminary results from a mechanical lung.

II. BACKGROUND

A. Lung Anatomy

Donor lungs are extracted in whole. A sample set of porcine lungs, connected to the EVLP system, is shown in Figure 1. Here, the visible lobes and fissures of the lung are labeled [7]. Missing in this case is the trachea, which is the tube connecting the lungs to the mouth and nose. The donor lungs are connected to the EVLP system's ventilator via an endotracheal intubation, as shown.

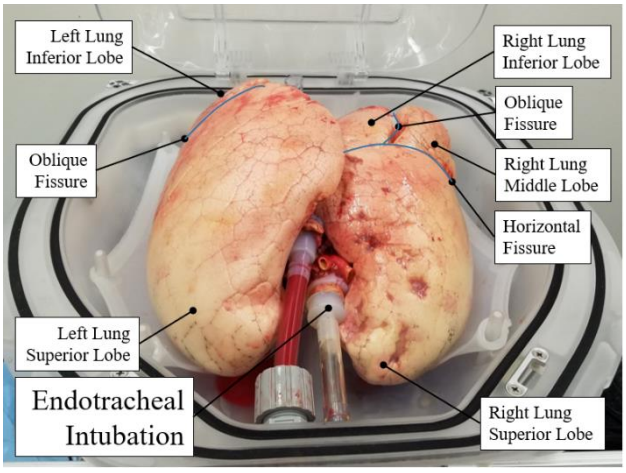

Figure 1. Ex-vivo lung perfusion prototype, donor lungs anatomy and endotracheal intubation (Courtesy of Tevosol)

1 TEVOSOL Inc., MITACS, CHIR

B. EVLP Device and Ventilation Measurements

Figure 2 displays the donor lungs placed within a pressure-sealed chamber encased by an optically transparent, semi-flexible cover. The EVLP device utilized in this research performs negative pressure ventilation (NPV), a technique for forced respiration by applying a net external pressure on the lungs [8]. NPV is implemented by regulating the pressures within the chamber and donor lungs. The difference between these pressures is the transpulmonary pressure. Currently, an airway sensor is used to monitor tidal volume and dynamic compliance.

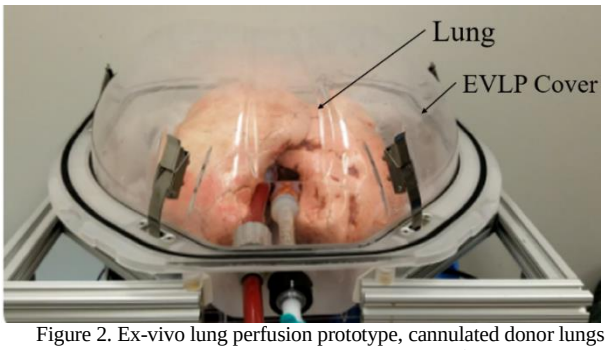

Figure 2. Ex-vivo lung perfusion prototype, cannulated donor lungs encased within pressure sealed chamber (Courtesy of Tevosol Inc.)

During normal respiration, lung volume follows a sinusoidal curve, which is measured by integrating the airway sensor flowrate measurements. In this respiratory cycle, tidal volume is the volume of air displaced between inhalation and exhalation [9]. Combined with the transpulmonary pressure measurements, the system can monitor dynamic compliance.

Dynamic compliance is a measure of the lung's elasticity. It is a vital metric for adjusting EVLP mechanical ventilation and is an indicator of lung health [10]. Conceptually, it is the rate of change of the lung volume with respects to the applied pressure. For NPV, it can be found using (1).

$$C_{dyn} = \frac{V_{te}}{TPP_e - TPP_i} \qquad (1)$$

where C_{dyn} is the dynamic compliance of the donor lungs. V_{te} is the exhalation tidal volume, and TPP_e, and TPP_i are the exhalation and inhalation transpulmonary pressures.

C. Volume Measurement using Computer Stereo Vision

Obtaining 3D measurements from 2D images has been a topic of research since the 1960s [11]. Many algorithms and camera configurations have been developed for a variety of applications, such as distance measurement of a scene using active stereo vision (ASV) [12]–[14]. Like eyesight depth perception, a pair of cameras can triangulate the distance of objects within a shared scene, which can be stored as a grayscale image called a depth map. This process can be improved by using a projector to emit a light pattern onto the scene, adding distinct points that are easier to identify and match between sets of images. To perform these computations, the camera system must be mathematically modelled to transform the measurements on a grid of pixels in the images into physical measurements.

Structured Light Plethysmography (SLP) is a non-invasive computer stereo vision method to measure patient tidal volume [15]. It reconstructs the surface shape of the patient's anterior chest wall during respiration. The patient's chest volume is measured as the space between the reconstructed surface and the patient's static posterior chest wall. Tidal volume is measured as the change in chest volume between the respective peaks at inhalation and exhalation [9], [16], [17]. SLP has been demonstrated to be as accurate at measuring tidal volume as the gold standard in clinical instrumentation [15], [18]. An approach like SLP can be applied to ex-vivo lungs within an EVLP device to measure tidal volume, dynamic compliance, and reconstruct the lung's surface shape.

III. METHOD

A. Experimental Setup

The proposed method has been developed using an Intel RealSense D435 camera system. Figure 3 displays the device, annotated to highlight the primary components: a depth sensor system comprised of two infrared cameras and an infrared projector, and a color camera. The device's onboard processor produces 3D measurements that can be accessed using a software development kit (SDK). The SDK is compatible with several programming languages, including MATLAB. The manufacturer also provides programs for accessing measurements, calibration, and evaluating measurement accuracy.

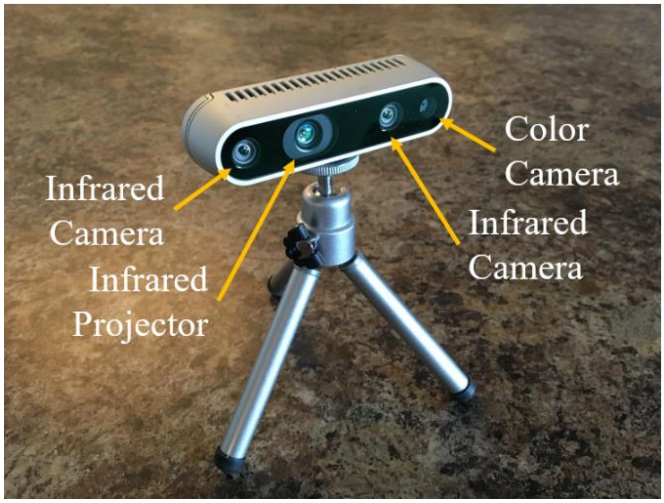

Figure 3. Intel RealSense D435 infrared active stereo and color camera

The camera system was suspended above a 1 L mechanical lung using a tripod, mounts, and a structural beam as seen in Figure 4. Data was recorded from the camera to a laptop. The EVLP ventilation was regulated on an independent system developed by Tevosol.

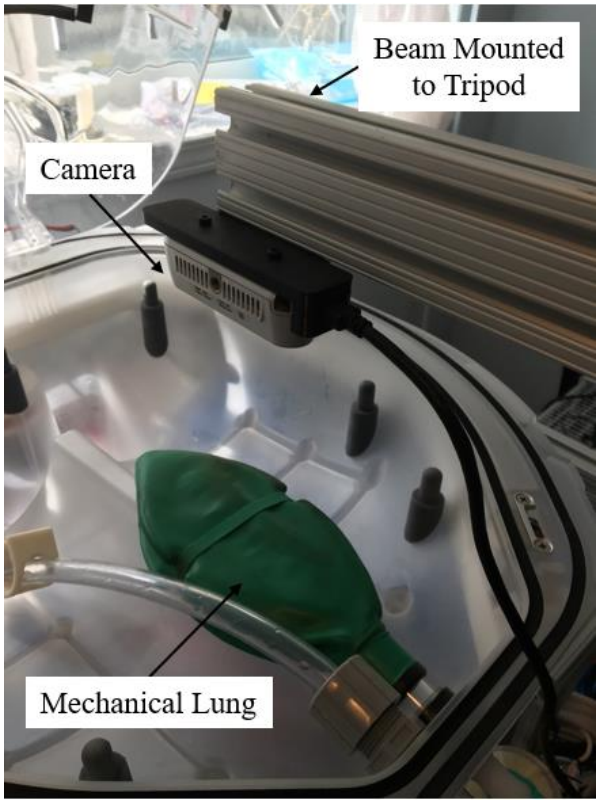

Figure 4. Positive pressure ventilation of mechanical lung with D435 camera system mounted above using T-slot aluminum and tripod.

B. Calibration

Typically, the well-known pinhole model is used for computer vision methods. This requires a calibration step to obtain the intrinsic, extrinsic, and distortion coefficients, collectively referred to as the camera parameters. In this process, images of a checkerboard pattern calibration plate are captured to solve for the camera parameters [19]–[21].

The D435 was calibrated using the Intel Realsense Dynamic Calibrator software to evaluate the extrinsic parameters [22]. The intrinsic parameters and distortion coefficients are set by the manufacturer.

The Intel Realsense Depth Quality Tool software was used to measure four metrics of calibration accuracy [23]. The D435 was positioned 1534mm above level ground, and the measurements were computed for a rectangular region of interest (ROI) 40% the size of the depth maps. Fill rate is a ratio of the valid to invalid pixels with depth measurements. The Z-Accuracy is the error between the measured ground truth distance and average distance. The Plane Fit RMS Error is a measure of the surface flatness and the Subpixel RMS Error is an empirical metric. Respectively, the metrics were measured to be 100%, -0.03%, 0.33% and 0.00 pixels. The manufacturer recommends re-calibration if the Z-Accuracy within 2 meters is above 2%, however the recorded metrics indicate that the D435 was more than adequately calibrated prior to data acquisition [23].

C. Data Acqusition

Depth map videos of the mechanical lung during ventilation were recorded using the Intel Realsense Viewer software as shown in Figure 5.

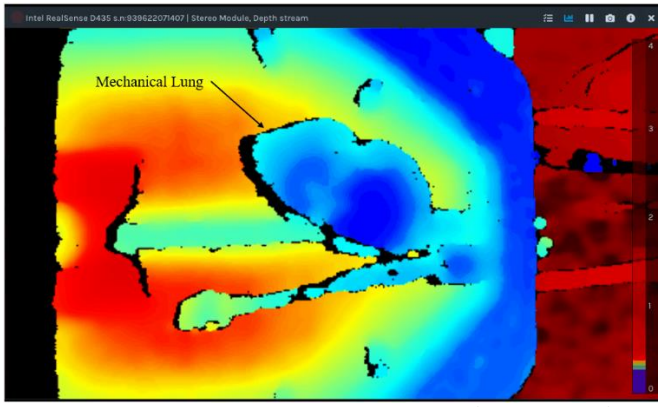

Figure 5. Histogram equalization visualization of a depth map of a mechanical lung during positive pressure ventilation.

Data was obtained for nine experiment configurations, with three different camera heights and ventilation flow rates. Ventilation flow rate was used to indirectly control tidal volume. Approximately 5 minutes of data was recorded for each configuration. Additionally, the ventilation settings were recorded with respect to time, including flow rate and pressure. All other conditions, such as camera exposure, other ventilation settings, and sampling rate remained constant. The depth map resolution was 480 x 848, sampling rate was 30 fps, and the mechanical lung was ventilated at a rate of 8 breaths per minute.

D. Image Processing

To improve measurements, the recorded depth maps were pre-processed using the Intel Realsense SDK digital image filters [24]. These enhanced depth maps were contrast adjusted, then segmented to identify the mechanical lung. The border between the mechanical lung and background were identified using a Sobel filter. The depth map masks are constructed from the area enclosed by the border. The result is a superimposed segmentation mask over the original depth map as shown in Figure 6. This enables the isolation of the mechanical lung from the depth map for further computations.

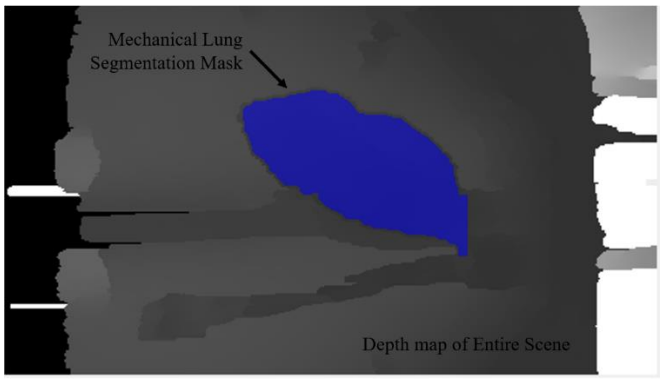

Figure 6. Grayscale depth map of the experiment scene overlayed with a segmentation mask to identify the mechanical lung.

The mechanical lung in the depth map is transformed into a collection of 3D points in physical space, also called a point

cloud. This transformation is called deprojection, which uses the known camera parameters to translate measurements in pixel space to physical space relative to the camera. The mechanical lung in Figure 6 was deprojected into the point cloud shown in Figure 7.

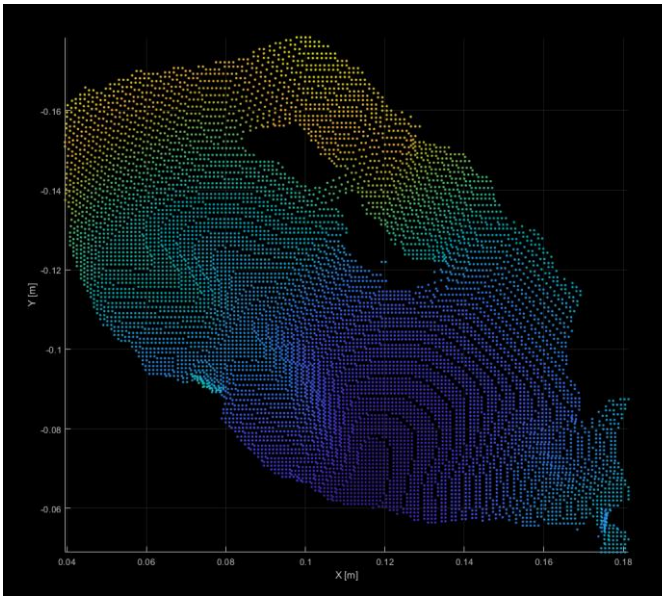

Figure 7. Point cloud of the mechanical lung surface.

To reconstruct the mechanical lung's surface, the point clouds are used to create Delaunay triangulation surface meshes. A 2D mesh is generated within the outline of each point cloud. The z-coordinate for each 2D mesh node is interpolated from the point cloud, creating a 3D surface mesh. Also, the pointcloud must be rotated 180° and translated the height of the camera to measure the height of the surface, instead of the distance to the camera. A Delaunay surface mesh of the mechanical lung is shown in Figure 8, where height of each element is visualized as a heatmap.

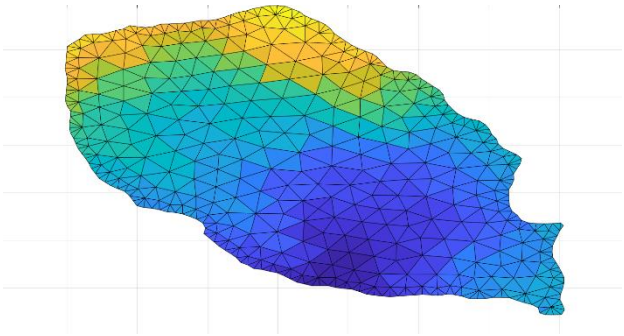

Figure 8. Delaunay triangulation surface mesh of mechanical lung, distance to camera displayed as a heatmap.

IV. Results

A. Lung Volume and Tidal Volume

As an initial approach, the Divergence Theorem is used to integrate the volume between the anterior and posterior lung walls [15]. This method is a simplification of volume measurement between surfaces of a tetrahedron [25].

$$\int_T (\vec{F} \cdot \hat{n}) dS = (\vec{u}\ x\ \vec{v}) \cdot \left[\left(\frac{p_0}{2} + \frac{\vec{u}+\vec{v}}{6} \right) \cdot \hat{k} \right] \hat{k} \qquad (2)$$

De Boer *et al* [15] proposed the closed-form solution to the volume integration of a single triangle element, as seen in (2). The surface vectors *u* and *v* are found as the difference between surface points, p_1-p_0 and p_2-p_0, where *k* is the basis vector for z cartesian coordinates.

$$V = \frac{1}{6} \sum_{i=1}^{N_T} [(\vec{u_i}\ x\ \vec{v_i}) \cdot (T_{i0z} + T_{i1z} + T_{i2z})] \qquad (3)$$

Equation (3) is the discretized form of (2) that was implemented for volume calculation. T_{i0z}, T_{i1z}, and T_{i2z} are the *z* coordinates of points p_0, p_1, and p_2 that form the mesh element T_i.

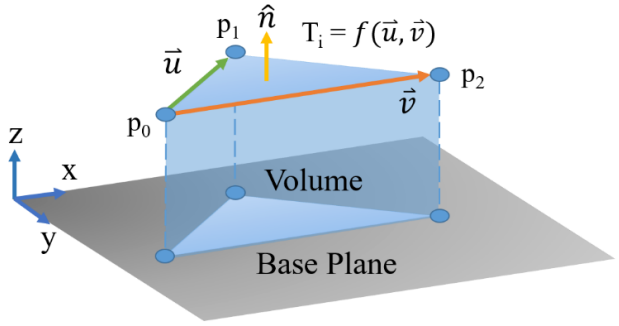

Figure 9. Schematic of parameterized triangular surface mesh for volume integration using the Divergence Theorem.

Figure 9 is a schematic for the volume integration of a single triangular surface mesh element above a plane. The three points of the triangular mesh *Ti* are used to create the vector parameters *u* and *v*. The element's normal vector is the cross product of these two parameters. Volume integration is performed for each triangular element of the surface mesh, and the sum is taken as the lung volume. This process is repeated for each set of images captured over time, which produces a volume signal as seen in Figure 10. The measured volume is plotted alongside the ventilation airway flow rate to visualize the timing relationship between the measured physical shape change and ventilation.

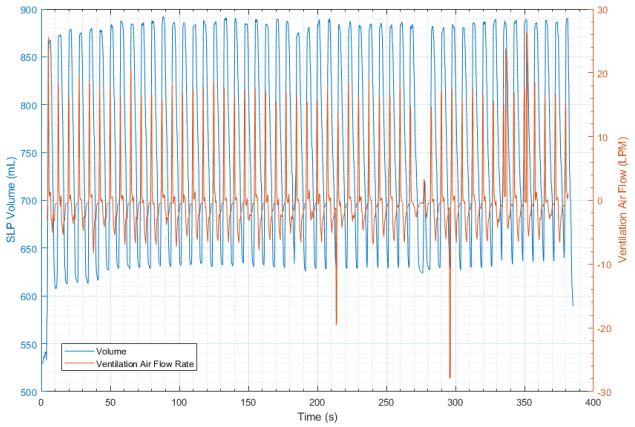

Figure 10. Volume of mechanical lung measured using camera, synchronized with ventilation airway flowrate.

The tidal volumes can be computed using the inflection points of the volume signal to identify the start and end of each breathing period as shown in Figure 11. Each breathing period is segmented into an inspiratory and expiratory phase. The tidal

volume measurements are compared to the breath-by-breath volumes integrated from the EVLP airflow. A moving average is applied to the EVLP tidal volumes.

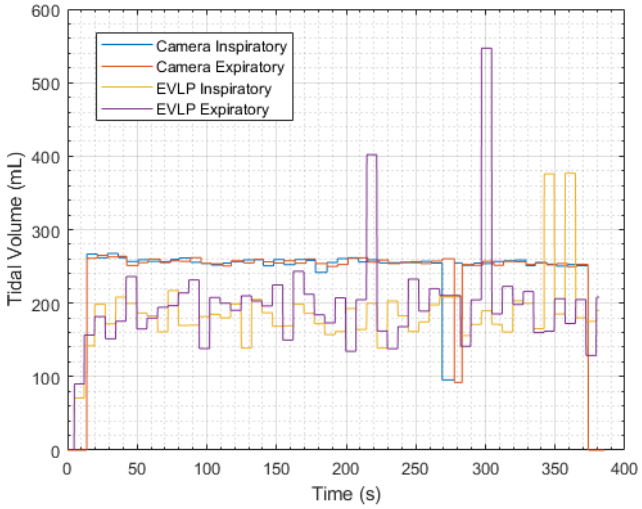

Figure 11. Inspiratory and expiratory tidal volume of ventilated mechanical lung measured using camera and airway flow rates.

B. *Dynamic Compliance*

For positive pressure ventilation, the dynamic compliance was found using the expiratory tidal volumes measured by the EVLP, and pressure difference between inflection points (peak inspiratory pressure and positive end-expiratory pressure). This is like equation (1) for negative pressure ventilation. The dynamic compliance measurements from camera and the EVLP airflow are compared in Figure 12.

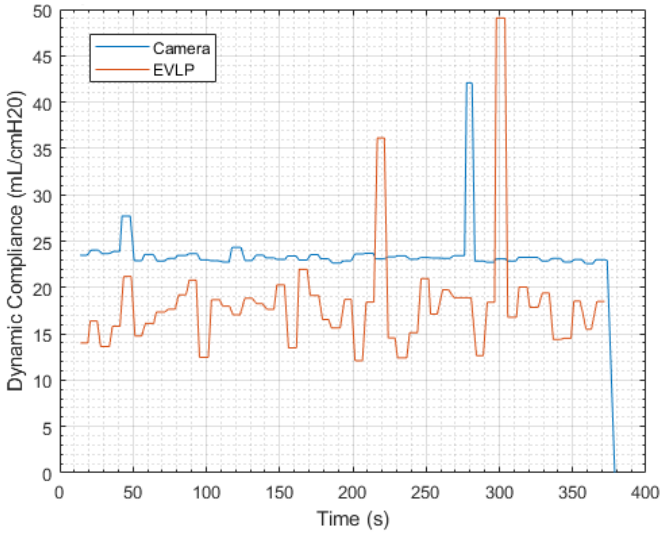

Figure 12. Dynamic compliance measured using camera and airflow.

V. Discussion

A. *Sources of Error and Observations*

The agreement between camera and EVLP tidal volumes were analyzed using the Bland and Altman method. For both inspiratory and expiratory tidal volumes, the methods were found to have a statistically significant bias, as the line of equality is not within the mean confidence intervals as seen in Figure 13 and Figure 14.

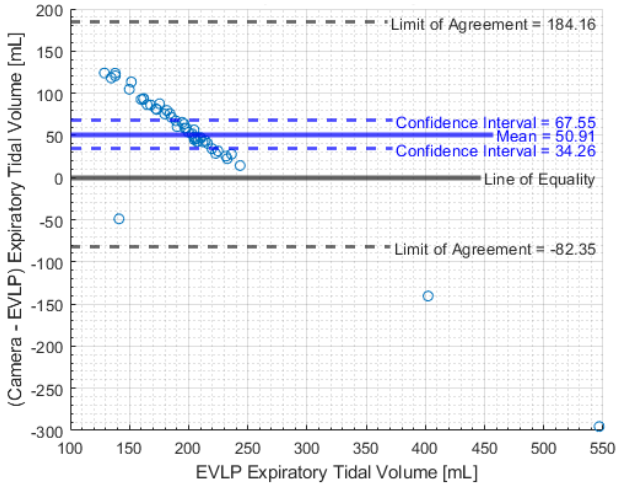

Figure 13. Expiratory tidal volume difference between camera and EVLP measurements in a Bland and Altman method plot.

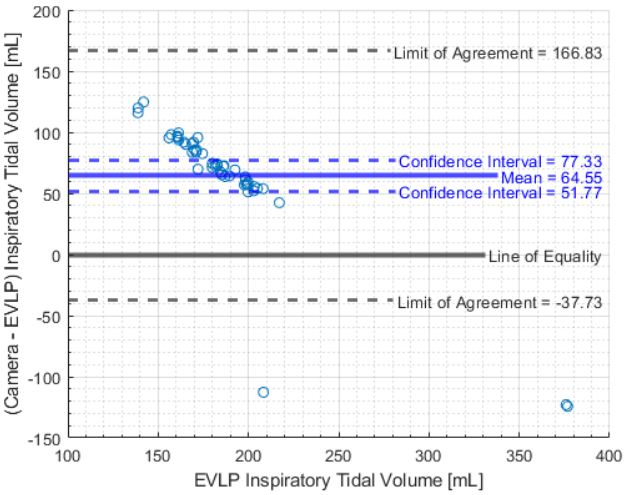

Figure 14. Inspiratory tidal volume difference between camera and EVLP measurements in a Bland and Altman method plot.

The camera tidal volumes and dynamic compliance are greater than the EVLP measurements. This error could be due to the bottom surface of the mechanical lung inflating and raising up the top surface. This would result in larger measured volumes, especially at peak inflation. . Also, the mechanical lung is not hollow, it is filled with foam. This could cause the EVLP to measure smaller volumes than the volume contained within its shell, as the foam takes up space. The accuracy of each processing step may be a factor. Lastly, the inconsistency of the airflow may be a source of error.

Notably, the volume signal is synchronized with the airway flow rate. However, there is a slight time delay between the start of each breath based on the tidal volumes. Finally, the camera measurements are more consistent than the ventilation measurements as shown in Figure 11 and Figure 12. The inspiratory and expiratory tidal volume standard deviations respectively of the camera are 23.85 and 24.18, while the EVLP are 44.24 and 66.68 mL.

B. *Future work*

A major concern is correcting for warpage and false matching due to the EVLP reflective cover. Without corrections, the curvature and reflectivity of the cover can cause false stereo image matching and obstruct measurements of the ex-vivo lung. The infrared light projection further complicates this issue. Calibration with the cover could correct for image warpage, and digital filters could remove the glare from the raw infrared images. Also, careful environmental lighting, positioning of the camera, and a polarizing lens could mitigate this issue [26].

The current method segments the entire lung. However, it would be more informative if the method measured the individual lung lobes. This would require segmentation of the lung lobes, potentially by identifying the lung fissures using digital filters or an aligned color camera. A global tidal volume and dynamic compliance could be calculated from the sum and average of these lung lobe specific measurements.

The shape of the mechanical lung was reconstructed as a 3D surface mesh, but not verified. It could be treated and analyzed like a scalar field to identify regions of overinflation and lung de-recruitment, smaller than the lung lobes. Potentially, the gradient and divergence of the height of the surface mesh could act as metrics to identify these 3D peaks and troughs.

VI. CONCLUSION

A non-invasive computer stereo vision method for monitoring donor lung shape change, tidal volume, and dynamic compliance has been outlined for use during EVLP. These measurements could be useful tools for evaluating transplant viability.

ACKNOWLEDGMENT

The authors acknowledge the support of their sponsor company Tevosol Inc. for their technical guidance and financial support and the financial support of the MITACS Acceleration and CHRP (CHIR / NSERC) programs.

REFERENCES

[1] M. T. Buchko *et al.*, “Clinical transplantation using negative pressure ventilation ex situ lung perfusion with extended criteria donor lungs,” *Nat. Commun.*, vol. 11, no. 1, pp. 1–5, 2020, doi: 10.1038/s41467-020-19581-4.

[2] J. Possoz, A. Neyrinck, and D. Van Raemdonck, “Ex vivo lung perfusion prior to transplantation: An overview of current clinical practice worldwide,” *J. Thorac. Dis.*, vol. 11, no. 4, pp. 1635–1650, 2019, doi: 10.21037/jtd.2019.04.33.

[3] M. Cypel *et al.*, “Normothermic Ex Vivo perfusion prevents lung injury compared to extended cold preservation for transplantation,” *Am. J. Transplant.*, vol. 9, no. 10, pp. 2262–2269, 2009, doi: 10.1111/j.1600-6143.2009.02775.x.

[4] A. S. I. Andreasson, J. H. Dark, and A. J. Fisher, “Ex vivo lung perfusion in clinical lung transplantation-State of the art,” *Eur. J. Cardio-thoracic Surg.*, vol. 46, no. 5, pp. 779–788, 2014, doi: 10.1093/ejcts/ezu228.

[5] X. Pan, J. Yang, S. Fu, and H. Zhao, “Application of ex vivo lung perfusion (EVLP) in lung transplantation,” *J. Thorac. Dis.*, vol. 10, no. 7, pp. 4637–4642, 2018, doi: 10.21037/jtd.2018.07.95.

[6] D. E. H. R. C. J. Loscalzo, “基因的改变NIH Public Access,” *Bone*, vol. 23, no. 1, pp. 1–7, 2011.

[7] J. D. Cooper *et al.*, “Technique of successful lung transplantation in humans,” *J. Thorac. Cardiovasc. Surg.*, vol. 93, no. 2, pp. 173–181, 1987, doi: 10.1016/s0022-5223(19)36439-6.

[8] L. Gattinoni *et al.*, “The future of mechanical ventilation: Lessons from the present and the past,” *Crit. Care*, vol. 21, no. 1, pp. 1–11, 2017, doi: 10.1186/s13054-017-1750-x.

[9] S. Motamedi-fakhr, R. C. Wilson, and R. Iles, “Tidalbreathing,” pp. 1–9, 2017.

[10] A. Slama *et al.*, “Standard donor lung procurement with normothermic ex vivo lung perfusion: A prospective randomized clinical trial,” *J. Hear. Lung Transplant.*, vol. 36, no. 7, pp. 744–753, 2017, doi: 10.1016/j.healun.2017.02.011.

[11] T. S. Huang, “Computer Vision: Evolution and Promise,” *Report*, 1997.

[12] N. Lazaros, G. C. Sirakoulis, and A. Gasteratos, “Review of stereo vision algorithms: From software to hardware,” *Int. J. Optomechatronics*, vol. 2, no. 4, pp. 435–462, 2008, doi: 10.1080/15599610802438680.

[13] E. Carmi and J. Vossoughi, “Geometrical Calculations with Stereo Vision,” pp. 1–4, 2015.

[14] C. Chen and Y. F. Zheng, “Passive and Active Stereo Vision for Smooth Surface Detection of Deformed Plates,” *IEEE Trans. Ind. Electron.*, vol. 42, no. 3, pp. 300–306, 1995, doi: 10.1109/41.382141.

[15] W. H. De Boer *et al.*, “SLP: A zero-contact non-invasive method for pulmonary function testing,” *Br. Mach. Vis. Conf. BMVC 2010 - Proc.*, pp. 1–12, 2010, doi: 10.5244/C.24.85.

[16] I. Levai, V. Sidoroff, and R. Iles, “An introduction to the non-invasive non-contact assessment of respiratory function,” *Respir. Ther.*, vol. 7, no. 5, p. 43, 2012.

[17] S. Motamedi-Fakhr *et al.*, “Evaluation of the agreement of tidal breathing parameters measured simultaneously using pneumotachography and structured light plethysmography,” *Physiol. Rep.*, vol. 5, no. 3, pp. 1–16, 2017, doi: 10.14814/phy2.13124.

[18] S. Motamedi-Fakhr *et al.*, “Evaluation of the agreement of tidal breathing parameters measured simultaneously using pneumotachography and structured light plethysmography,” *Physiol. Rep.*, vol. 5, no. 3, pp. 1–16, 2017, doi: 10.14814/phy2.13124.

[19] J. Salvi, X. Armangué, and J. Batlle, “A comparative review of camera calibrating methods with accuracy evaluation,” *Pattern Recognit.*, vol. 35, no. 7, pp. 1617–1635, 2002, doi: 10.1016/S0031-3203(01)00126-1.

[20] X. Chen, J. Xi, Y. Jin, and J. Sun, “Accurate calibration for a camera-projector measurement system based on structured light projection,” *Opt. Lasers Eng.*, vol. 47, no. 3–4, pp. 310–319, 2009, doi: 10.1016/j.optlaseng.2007.12.001.

[21] Z. Zhang, “A flexible new technique for camera calibration,” *IEEE Trans. Pattern Anal. Mach. Intell.*, vol. 22, no. 11, pp. 1330–1334, 2000, doi: 10.1109/34.888718.

[22] U. Guide, “Intel ® RealSense ™ Product Family D400 Series Calibration Tools,” no. July, 2020.

[23] Intel, “Camera depth testing methodology,” pp. 1–18, 2018, [Online]. Available: www.intel.com/design/literature.htm.

[24] A. Grunnet-jepsen and D. Tong, “Depth Post-Processing for Intel ® RealSense ™ D400 Depth Cameras,” *Report*, 2018, [Online]. Available: https://en.wikipedia.org/wiki/Moving_average.

[25] C. Engineering and F. Avenue, “IN MESH REPRESENTATION Cha Zhang and Tsuhan Chen,” *Virtual Real.*, pp. 1–4, [Online]. Available: http://chenlab.ece.cornell.edu/Publication/Cha/icip01_Cha.pdf.

[26] J. Sweetser and A. Grunnet-jepsen, “Optical Filters for Intel ® RealSense ™ Depth Cameras D400,” p. 27.